A Method Based on Measured Boundary Conditions for Reconstructing the Magnetic Field Distribution of an Electromagnetic Mechatronic System

Liang Hu, Kok-Meng Lee, *Fellow, IEEE*, and Xin Fu

***Abstract*—This paper presents a cost-effective method for reconstructing the magnetic field distribution (MFD) from measured data of an electromagnetic mechatronic system (EMS). MFD predictions and measurements for model-based force/torque calculation and magnetic sensors are common problems in EMS where permanent magnets (PMs) and/or electromagnets are employed. In this method, the MFD is reconstructed in the current-free space by solving the Laplace's equation of a magnetic scalar potential with measured boundary conditions (BCs). The reconstruction method, which relaxes the assumption of known magnetic structures commonly made in the magnetic models for design analysis, requires only the normal component of the magnetic flux density on its boundary surface. Two practical applications are given to illustrate the reconstruction method. The first example illustrates the reconstruction of the MFD from published data of a spherical rotor with embedded PMs for a ball-joint-like motor, where the MFD is essential for the Lorentz force computation. The second example reconstructs the MFD in a circular pipe of an electromagnetic flowmeter, where the MFD is essential for the sensitivity computation. Both reconstructions have been experimentally validated by comparing the MFD against measured data. Both comparisons show excellent agreements. In addition, a gradient-based data distribution on MFD is also discussed to illustrate how the BCs are employed for the reconstruction process.**

***Index Terms*—Electromagnetic, flowmeter, magnetic field, measured boundary condition (BC), mechatronic system, reconstruction, spherical motor.**

I. Introduction

MAGNETIC fields have been widely used in a spectrum of electromagnetic mechatronic systems (EMSs), which include multi-DOF actuators [1], sensors [1]–[3], precision motion stages [4], bearing [5], [6], fluid velocity probe [7], [8], flowmeter [9], and MRI devices [10]. The inherent existence of the 3-D magnetic field distribution (MFD) in the EMS, however, is often underexploited due to the difficulty to experimentally characterize (or to perform periodic calibration) the 3-D field once the system is fabricated. Traditionally, MFD measurements primarily rely on single-point magnetic sensors (such as a Hall sensor). Although single-point sensors are inexpensive and capable of very high-resolution measurement, their uses to cover the whole working space require an additional positioning device [11], [12]. Thus, 3-D MFD measurements are generally tedious, time-consuming, and costly. Recent advance in mathematical modeling, computational algorithms, and mechatronics (that integrate computer, communication, and control) have provided a rationale basis to exploit computational models as a computer-aided experimental approach to characterize the MFD of an EMS. For this reason, this paper presents a cost-effective computational method to derive the MFD from measured data on its boundary surface.

MFD predictions and measurements for model-based force/torque calculation and magnetic sensors are common problems in EMS where PMs and/or EMs are employed. MFD problems may be formulated in two opposing ways (or forward and inverse models). The forward model analyzes the effect of a given cause. Conversely, the inverse model defines the causes of a prescribed or measured effect; in mechatronics, it addresses two important MFD subproblems. The first subproblem (also popularly known as design optimization) is to seek a solution (for the purpose of designing a device) in order to meet a specified behavior and/or an optimal performance. The second subproblem (also known as calibration, system identification, and parameter estimation) aims at reconstructing information on a mathematical model of the system from given data. Unlike the first subproblem where the solution may not exist because data are assumed arbitrary in synthesis, the second subproblem uses data from measurements, and is the focus of this paper.

Although MFD problems have been studied for decades, most traditional methods have focused on solving the forward model for a given design. For systems with geometrically simple exciting units (such as circular and square air-cored coils [8], or orderly arranged PMs with known polarized magnetic strengths [11], Maxwell's equations can be appropriately simplified and analytically solved for the magnetic fields in the working space. These methods include the assumed flux path approximation [13], analytic methods [11], [14], dipole closed-form solutions [1], [15], and finite-element method [16], where the MFD was solved for calculating the torque of a 3-DOF spherical motor. More recently, interests to derive optimal synergy between electromagnetic and mechanical design have motivated a number of researchers to develop methods for computationally efficient design optimization [15], [17]–[19]

Manuscript received April 17, 2009; revised June 29, 2009; accepted August 6, 2009. Date of publication September 22, 2009; date of current version July 28, 2010. Recommended by Technical Editor W.-J. Kim. This work was supported in part by the National Basic Research Program (973) of China under Grant 2006CB705400, in part by the Key Industrial Program of Zhejiang Province of China under Grant 2008C01025-3, and in part by the Georgia Tech Foundation (2505E34).

L. Hu and X. Fu are with the State Key Laboratory of Fluid Power Transmission and Control, Zhejiang University, Hangzhou 310027, China (e-mail: cmeehuli@zju.edu.cn; xfu@zju.edu.cn).

K.-M. Lee is with the George W. Woodruff School of Mechanical Engineering, Georgia Institute of Technology, Atlanta, GA 30332-0405 USA (e-mail: kokmeng.lee@me.gatech.edu).

Color versions of one or more of the figures in this paper are available online at http://ieeexplore.ieee.org.

Digital Object Identifier 10.1109/TMECH.2009.2030795

and motion control applications [16], [20] where computation must be performed in real time.

Actual magnetic structures, however, may differ from the computer-aided design (CAD) models (due to fabrication tolerances and inherent nonlinear material properties). Physically accurate MFD, which is essential for model validation, system calibration, identification, and parameter estimation in an EMS, can be determined only from the measured data. The torque model of a three-DOF spherical motor was experimentally obtained in [20] to account for the effect of MFD using an energy-based lumped-parameter approach. The method [20] assumes that the electromagnetic structure of the system is known. More recently, dipole models have been developed for incorporating measured MFD data in the multi-DOF actuators and sensors [1], [15].

It has been shown in [7] and [12] that the magnetic field in the current-free working space around an electromagnetic velocity probe can be reconstructed using only the normal component of the magnetic flux density on the boundary surface. In [7] and [12], where numerical and analytical methods are provided, respectively, experimental realization of the MFD reconstruction was conducted for a specific velocity probe. This paper further develops the reconstruction method so that the method can be applied to a broader range of EMS applications, where the electromechanical energy conversion generally takes place in the field near, but outside, the physical region of the exciting units. The remainder of this paper offers the followings.

1) The paper presents a method based on measured boundary condition (BC) to obtain physically accurate (yet cost-effective) MFD from measured data in the working space. This method, which relaxes the assumption of known magnetic structures commonly made in the forward models or optimal design problems, only requires the normal component of the magnetic flux density on its boundary surface. Different from [7] and [12], where only Neumann BCs (NBCs) were used, the method presented here considers all kinds of BCs including Neumann, Dirichlet, and their combination. In addition, we highlight the mathematical insights, physical interpretations, and measurement considerations of typical BCs commonly encountered in EMS applications.
2) Two practical applications with relatively complex electromagnetic structures are given to illustrate the reconstruction method: a permanent magnet (PM) based spherical motor and an electromagnet (EM) flowmeter. For a spherical motor, the reconstructed MFD provides the basis for computing the magnetic torques from the Lorentz force equation. The MFD of an EM flowmeter provides the basis for computing its sensitivity (dry calibration) based on the electromagnetic flow-measurement theory [21]. Unlike an EM velocity probe [7] and [12] that measures the local velocity at a point inside a pipe, the EM flowmeter offers unobstructed measurements of the average velocity of the flow passing through the pipe. The reconstruction task is different from [7] and [12] in that the magnetic field inside the flowmeter is reconstructed from measured data on the inner surface of the pipe, but not outside of the probe surface.
3) The MFD reconstruction method has been validated in both applications (spherical motor and flowmeter) by comparing the reconstructed MFDs against measured data. As will be shown, both comparisons show excellent agreements.
4) The effect of reduced measured BC data (based on gradient information) on the MFD is discussed.

While the reconstruction method illustrated here is in the context of electromagnetic fields, the procedure introduced in this paper can be extended to other physical field (such as thermal and electrical) based mechatronic systems, as long as the field obeys similar governing equations (such as Laplace and Poisson equations) with measurable BCs.

II. Principle of the Reconstruction Approach

The term "reconstruction" is defined here as a coupled measurement–calculation approach that derives the magnetic field in a working space from measured data on its boundary surface. For a current free ($\mathbf{J} = 0$) working space, the magnetostatic field can be characterized by the Maxwell's equations as

$$\nabla \times \mathbf{H} = 0 \tag{1a}$$

and

$$\nabla \cdot \mathbf{B} = 0 \tag{1b}$$

where $\mathbf{H}$ and $\mathbf{B}$ are the magnetic field intensity and flux density, respectively. In this case, a magnetic scalar potential ψ can be defined, from which $\mathbf{H}$ and $\mathbf{B}$ are derived through the expressions (2a) and (2b), respectively

$$\mathbf{H} = -\nabla\psi \tag{2a}$$

and

$$\mathbf{B} = -\mu\nabla\psi \tag{2b}$$

where μ is the magnetic permeability of the material in the working spaces. According to (1b) and (2b), the potential ψ obeys the Laplace's equation as

$$\nabla^2\psi = 0. \tag{3}$$

In physics, any field whose potential obeys (3) is free and can be uniquely determined by the field condition on the boundary surface, which may take one of the three forms.

1) Dirichlet BC specifies the potential ψ at the boundary surface.
2) NBC specifies the derivative of ψ at the boundary surface.
3) Mixed BC specifies DBC in some boundary surfaces and *NBC* on the remainder.

In theory, any one form of the aforementioned BCs can be used to completely specify the field condition on the boundary surface for solving the Laplace's equation (3), and along with (2a) or (2b), the corresponding $\mathbf{H}$ or $\mathbf{B}$ field distributions in the working space can be solved mathematically. However, as will be discussed, the choice of appropriate BCs is often limited

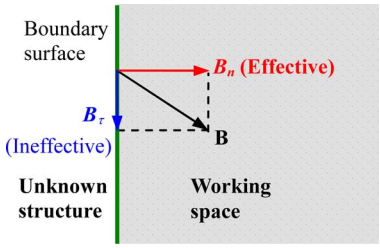

Fig. 1. Physical meaning of NBC.

by measurements, and thus, the following are implementation considerations for cost-effective field reconstruction.

1) The potential ψ is immeasurable in practice. With few exceptions (such as magnetically ground surface or remote far field), knowing its distribution on the boundary surface is nearly impossible. Thus, the DBC is commonly used to specify fields at magnetically ground surface or in infinite domains, where ψ can be reasonably approximated and arbitrarily set to zero.
2) As illustrated in Fig. 1, the magnetic flux density **B** at any point on the boundary surface can be decomposed into two components: normal B_n (positive for outflow from and negative for inflow into the working space) and tangential B_τ. As B_τ at the boundary does not enter the working space, thus it has no contribution to the field to be reconstructed. The normal component of the magnetic flux density $B_n = -\mu\partial\psi/\partial n$ is chosen as the NBC imposed on the boundary for reconstructing the field. Mathematically, (3) cannot be completely solved with NBC ($B_n = -\mu\partial\psi/\partial n$) due to the undeterminable constant ψ_0. However, ψ_0 is eliminated during the gradient calculation, and does not affect the determinations of **B** and **H** according to (2a) and (2b).
3) Without loss of generality, we assume that magnetic sensors (such as a Hall sensor) are available to measure the B_n distribution for the NBC on all the boundary surface (except the DBC at far field where $\psi = 0$).

The aforementioned points shows that the magnetic field **B** in a working space can be reconstructed from the measured B_n on its boundary surface. This reconstruction method that bases solely on the single-axis measurement greatly reduces the complexity and cost to obtain the **B** field in a finite working space.

The reconstruction method is best illustrated with examples. Two successful applications (with validation) with different magnetic structures are introduced in the following sections.

1) The first example is a PM-based spherical motor involving a mixed of *NBC* and *DBC* for the reconstruction.
2) The second example is an electromagnetic flowmeter using only measured B_n data as the *NBC* for the whole boundary.

In both examples, the Laplace's equation (3) is numerically solved for the magnetic scalar potential ψ using finite-element method. For this, the commercial software COMSOL Multiphysics is employed on an IBM System X3850M2 (four-way quad-core 2.4-GHz CPU, 64-GB RAM) to reach the solution with relative tolerance of 1e−6.

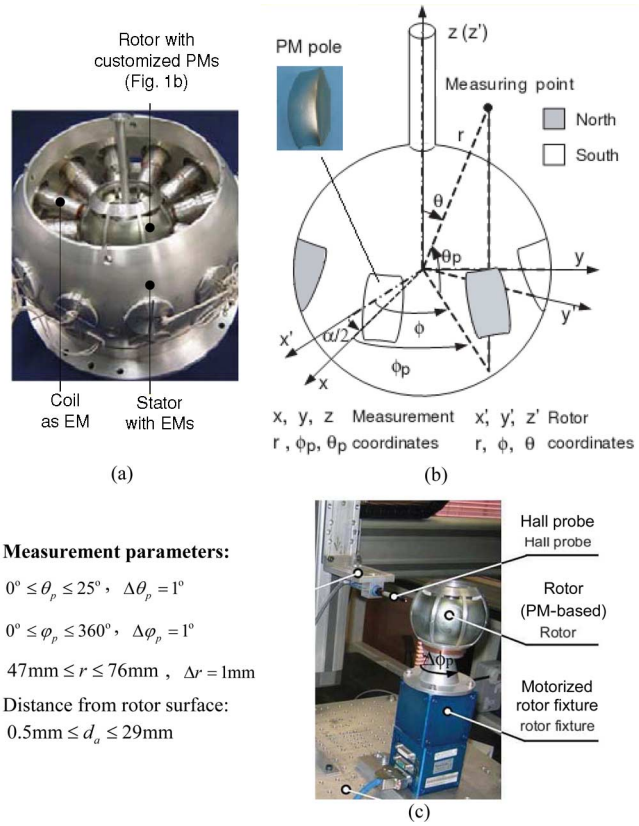

Fig. 2. Schematics illustrating the measurement (adapted from [11]). (a) Spherical motor. (b) Rotor with customized PMs. (c) Measuring device.

III. Magnetic Field of a Spherical Motor

Design and control of a multiaxis electromagnetic actuator or sensor require a good understanding of its magnetic field. Prior research on spherical motors has focused on developing analytical methods that offer an effective means to predict the magnetic field for design analysis [11], [19]. For model identification or calibration, it is desired that the magnetic field of the device can be reconstructed experimentally.

A. Experimental Setup

Fig. 2 shows the spherical rotor [11] (with eight customized-shaped PMs evenly along the "equator" of 46.5 mm radius) of an iron-free PM-based spherical motor. In a spherical motor [see Fig. 2(a)], the ball-like rotor is concentrically supported by means of a bearing inside a hollow spherical stator with strategically positioned stator coils as EMs. Torque, which can be calculated from the Lorenz force equation, is generated as current inputs flow through the stator coils in the magnetic field. As shown in [1], the Lorenz force calculation involves modeling only the flux density **B**-fields of the PMs, as the current density is directly used in the calculation. Thus, only the PM-embedded rotor [see Fig. 2(b)] is considered here for clarity in illustrating the reconstruction.

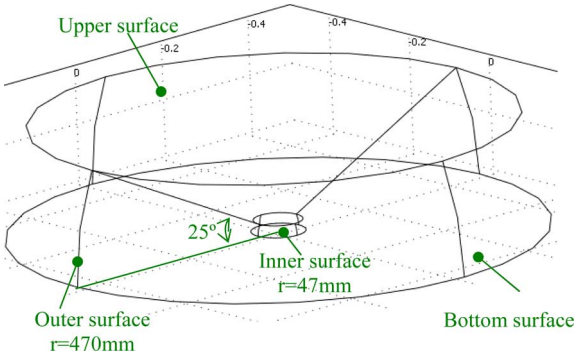

Fig. 3. Calculation model.

TABLE I
BCs IN CALCULATION MODEL (SPHERICAL MOTOR)

Surfaces	Boundary conditions	
Inner surface	*NBC*	Measured $B_r = -\mu\partial\psi/\partial r$ at d_a=0.5mm
Outer surface	*DBC*	ψ=0 at far field
Bottom surface	*NBC*	$B_n = -\mu\partial\psi/\partial n = 0$
Upper surface	*NBC*	$B_n = -\mu\partial\psi/\partial n = 0$

Experimental data and analytical solutions for the system are available in [11] and [19], and thus, this example provides a good basis for illustration and validation. While the detailed geometry of the PM-based spherical motor and the effect of its PM shape on the torque performance can be found in [11] and [19], the magnetic structure of the rotor is assumed unknown in the field reconstruction. Along with the measurement parameters, the setup used in measuring B_r (equal to B_n on spherical surface, which is the radial component of the magnetic flux density) in s(r, θ_p, φ_p) is shown in Fig. 2(c), where B_r is measured with a Hall probe driven by a three-axis stage. The published data are used directly as BCs in the reconstruction; no additional measurement was made.

B. Boundary Conditions

As shown in Fig. 3, the boundary surface is divided into four areas with the *mixed-BCs* specified in Table I. The measured B_r at $d_a = 0.5$ mm (where d_a is the distance from the rotor surface), as shown in Fig. 4, is imposed as a *NBC* on the inner surface. A zero *DBC* ($\psi = 0$) is imposed on the outer surface (with a radius ten times larger than that of the inner surface) to approximate the infinite far field. The bottom surface is the plane of symmetry, and thus, a zero *NBC* is imposed on it. It is worth mentioning that as measured B_n data at the upper surface are not available, a zero *NBC* is assumed as an approximation that the magnetic field in the space $\theta_p \geq 25^\circ$ is relatively small.

C. Results and Discussions

With the BCs specified in Table I, (3) is numerically solved using COSMOL. The model is meshed by 272 946 tetrahedral elements, and 389 233 DOFs are calculated. The computation took 224 s. The reconstructed **B** field is 3-D; a sample plot characterizing the **B** field at the bottom surface is shown in

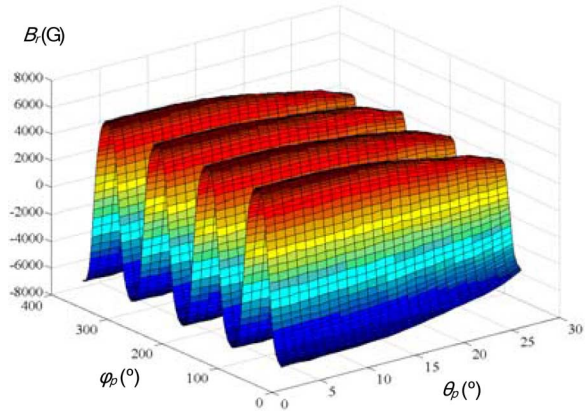

Fig. 4. Measured B_r on the surface $d_a = 0.5$ mm used as NBC [11].

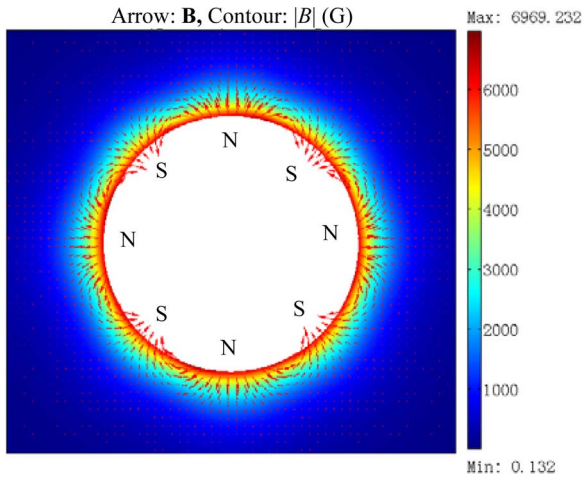

Fig. 5. Reconstructed **B** on the bottom surface.

Fig. 5. As expected, the field is periodic in the φ_p direction (due to the alternate PM magnetizations), and is strongest in the domain near the rotor surface where magnetic energy (as a media for electrical-to-mechanical conversion) is stored in the air gaps between PMs and stator EMs in the spherical motor [13], [20].

The approach is validated by comparing the reconstructed B_r distribution against measured data at $d_a = 2.5$ mm in Fig. 6(a) with the differences highlighted in Fig. 6(b). The reconstructed magnetic field well agrees with the original data (with an average maximum difference of about 3.6%) in the range of $0^\circ \leq \theta_p \leq 20^\circ$; this relatively small difference could be due to the unavoidable Hall probe positioning errors. Primary discrepancies are in the domain near $\theta_p = 25^\circ$ (with a maximum error of 23% at $\theta_p = 25^\circ$) due to the assumption $B_n = 0$ at the upper surface. Clearly, it can be greatly reduced if additional B_n measurements are obtained on this surface. As illustrated in next example, if all the BCs are obtainable, the reconstruction error will be quite small.

Once the MFD is reconstructed, it can be used to compute the torque model of the spherical motor [1], [11], and for parameter estimation and motion control [16].

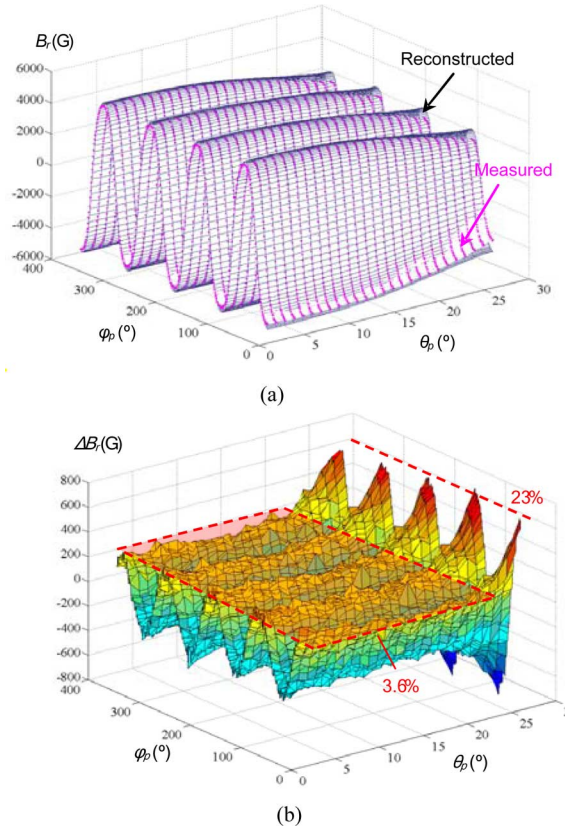

Fig. 6. Reconstructed fields at $d_a = 2.5$ mm. (a) Comparison between reconstructed and measured fields. (b) Computed difference.

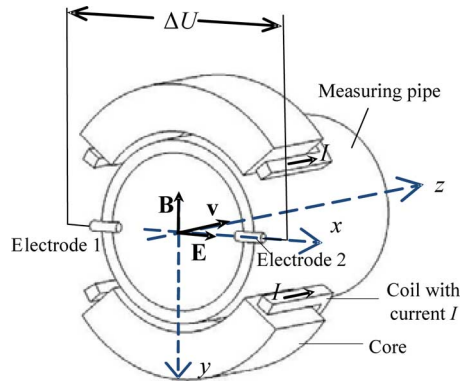

Fig. 7. Inner structure of electromagnetic flowmeter.

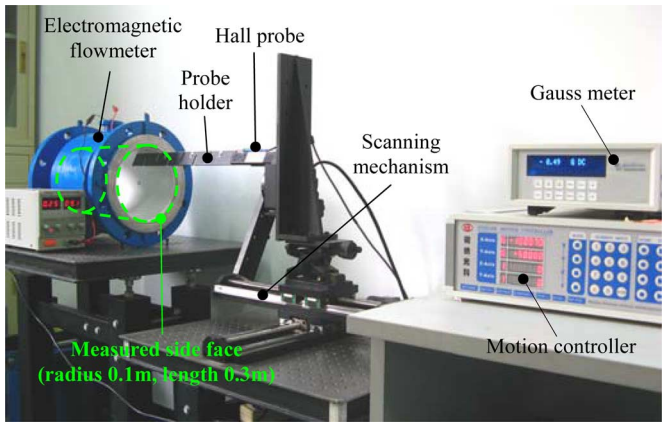

Fig. 8. Magnetic scanning device.

IV. Magnetic Field of a Electromagnetic Flowmeter

Fig. 7 shows an electromagnetic flowmeter, where the induced voltage ΔU is a function of the flow velocity **v** and the magnetic flux density **B** [21]. The flowmeter consists of a measuring pipe and a magnetic unit that excites an induction (between the electrodes as conductive liquid moves through the magnetic field) through a pair of EMs. Through measuring the magnitude of the induced voltage, the flow velocity can be determined from the Faraday's law of electromagnetic induction. The actual flowmeter consists of other components (such as yoke, shield layer, sailing layer, and signal lead channel, not shown in Fig. 7). However, the reconstruction of the magnetic field in the cylindrical pipe does not require the knowledge of the magnetic structure.

A. Measurement Setup

To provide the necessary *NBC* of the measuring pipe for solving the Laplace's equation (3), the normal component of the magnetic flux density distribution on the boundary surfaces is measured using a Hall probe, as shown in Fig. 8. To ensure that the whole magnetic field is calculated, two extended cylinders are added in the upstream and downstream, as illustrated schematically in Fig. 9.

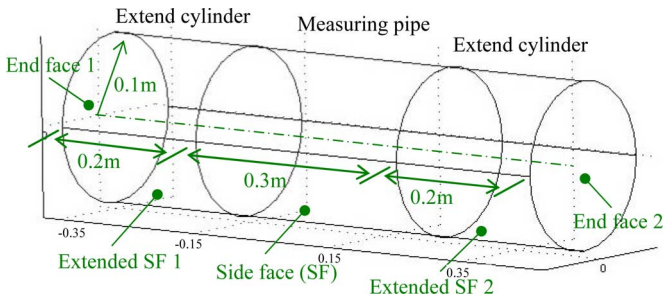

Fig. 9. Calculation models.

To automate the data collection and ensure a high measuring accuracy, a computer-controlled scanning servomechanism is designed to position the Hall probe on the aluminum holder:

1) Located near the end of the probe (monitored by the gauss meter), the diameter of Hall effect area is about 1 mm. Only the average value of the normal **B** component passing through this small area is measured.
2) Controlled by a motion controller, the rotational and translational resolutions of magnetic scanning device are 0.005° and 5 μm, respectively.
3) The gauss meter and motion controller along with a scanning program that monitored the autoscanning procedure are controlled by a host computer.

TABLE II
BCs IN CALCULATION MODEL (FLOWMETER)

Surfaces	Areas covered	NBC
Side face (SF)	$r = 0.1\text{m}, \quad -0.15\text{m} \le z \le 0.15\text{m}$	Measured $B_r(\theta, z)$
Extended SF 1	$r = 0.1\text{m}, \quad -0.35\text{m} \le z \le 0.15\text{m}$	B_r=0
Extended SF 2	$r = 0.1\text{m}, \quad 0.15m \le z \le 0.35m$	B_r=0
End face 1	$z = -0.35\text{m}, \quad 0\text{m} \le r \le 0.1\text{m}$	B_z=0
End face 2	$z = 0.35\text{m}, \quad 0\text{m} \le r \le 0.1\text{m}$	B_z=0

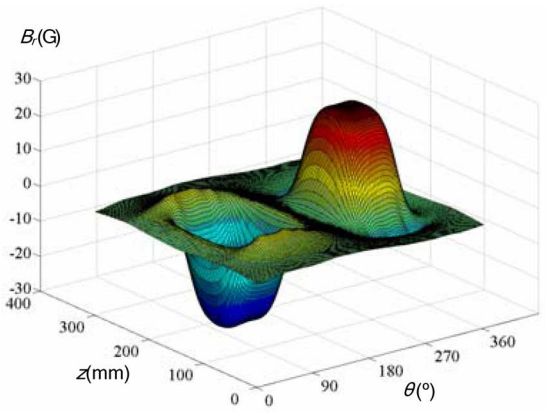

Fig. 10. Measured *NBC*, $B_r(\theta, z)$ on the surface of the pipe (measuring range $\theta = 0°$ to 360°, $z = 0$ to 300 mm, and measuring steps $\Delta\theta = 3°$ and $\Delta z = 2$ mm).

With the aforementioned design, the maximum measuring error of the readings is within $\pm 0.20\%$.

B. Boundary Conditions

The boundary surface is divided into five areas, for each of which an *NBC* is assigned. As listed in Table II that summarizes the BCs, only the $B_r(\theta, z)$ distribution (where the subscript "r" denotes the radial direction normal to the pipe surface) on the inner surface of the measuring pipe is measured. With five measurements taken at each point, a total of 18 000 points (in steps of $\Delta\theta = 3°$ and $\Delta z = 2$ mm) were measured in about 2.5 h. The measured B_r distribution is shown in Fig. 10.

C. Results and Discussions

With the *NBCs* given in Table II, the magnetic field was reconstructed numerically by solving (3) with (2a) and (2b), which took 229 s to compute a solution. The model is meshed by 178 234 tetrahedral elements, and 245 483 DOF are calculated. A sample of the reconstructed field **B** on the x–y plane (where two electrodes locate) is plotted in Fig. 11. The plot shows that the magnitude of **B** is smaller in the area near the electrodes, which is a design feature of the electromagnetic flowmeter to reduce the effect of the distorted flows.

To evaluate the reconstruction accuracy, we compare the reconstructed B_y (a major effective component of **B**) along the x-axis (line connecting the two electrodes) and z-axis (pipe axis) against the experimentally measured data in Figs. 12 and 13. Within the positioning tolerance, the comparisons that show

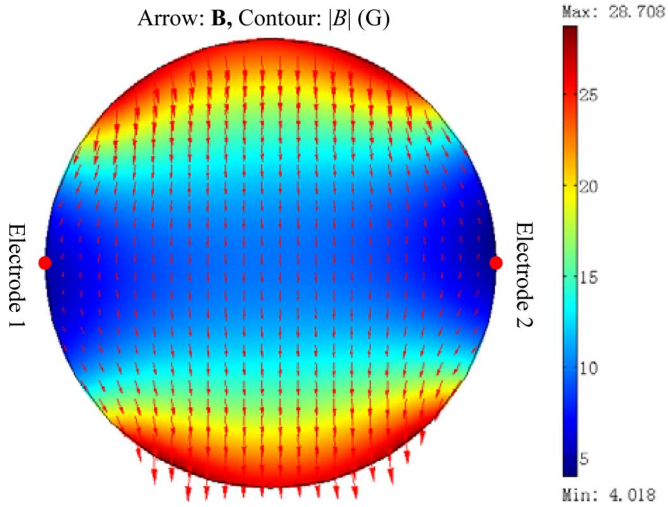

Fig. 11. Reconstructed **B** at $z = 150$ mm (where two electrodes are located).

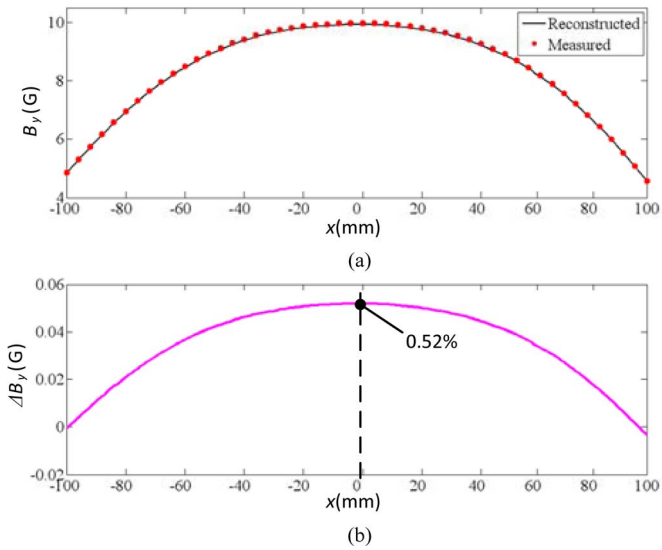

Fig. 12. Reconstructed fields on x-axis. (a) Comparison between reconstructed and measured fields. (b) Computed difference.

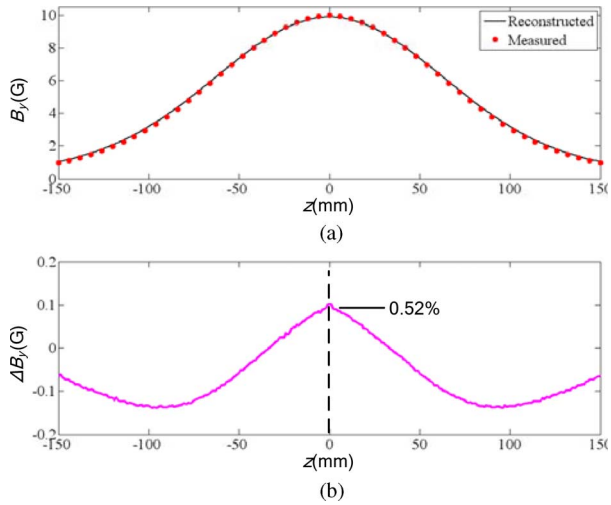

Fig. 13. Reconstructed fields on z-axis. (a) Comparison between reconstructed and measured fields. (b) Computed difference.

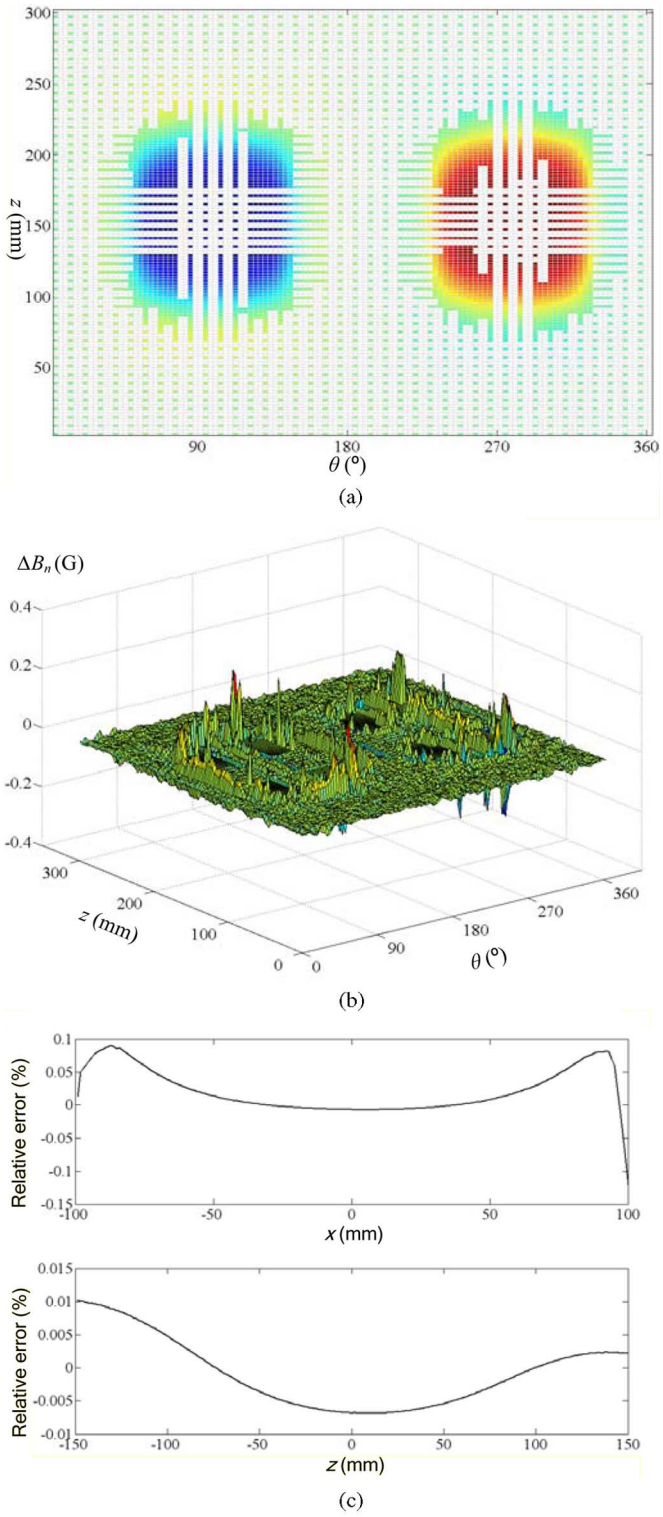

Fig. 14. Effect of gradient-based data distribution (EMF). (a) Data distribution (4526 points). (b) Relative error (gradient-based 4526 versus uniform 18 000) of BC. (c) Relative error (gradient-based 4526 versus uniform 18 000 points) of reconstructed B_y MFD on x- and y-axis.

excellent agreement (in the order of 0.5% difference) validate this reconstruction approach. As expected, the smallest errors occur at the boundary where measured data are available, and propagate toward the center.

V. Gradient-Based Data Distribution on MFD

In Sections III and IV, a dense set of equally spaced measurements (9360 points for the spherical motor and 18 000 points for the electromagnetic flowmeter, respectively) was used in reconstructing the magnetic field. These high-resolution data not only validate the reconstruction method, but also provide a basis to investigate the effects of data size and their distribution on the calibration errors, as well as a basis for benchmark comparison in the future.

Data collection is tedious, and is the most time-consuming part of the reconstruction process. For the flowmeter (Section IV), a single measurement took 0.5 s and the whole BC measurements took 2.5 h. In contrast, the MFD computation with FEM only used less than 4 min. In practice, it is desired that reconstruction can be performed with a small set of measurements for specifying the BCs. The simplest way to investigate this effect is to uniformly decrease the measurements in the whole boundary surface. However, if B_n values are relatively constant in certain local regions, this method is inefficient since extra data in constant B_n regions do not help to improve the overall calibration, but simply require longer measurement time.

A better alternative is to base decisions on the gradient of the magnetic field on the BC surface to select points for measurements. In other words, points with B_n gradient value higher than a threshold are kept, but when the gradient is smaller than the threshold, only one in every m number of points is retained. Additional points are calculated from measured data using interpolation. To best illustrate the scheme, the MFD of the flowmeter is recomputed as a basis for comparison. The results are given in Fig. 14.

Fig. 14(a) shows the selected 4526 points (based on a threshold of 0.5 G per step and $m = 3$) to specify the BCs for reconstructing the MFD, where a step is defined here as 2 mm in the z direction and 3° in the θ direction. As in previous sections, color characterizes the magnitude of B_n in Fig. 14(a). The FEM uses the same number of points in COMSOL numerical computation (but only 4526 of the 18 000 BC points are actually measured, while the remaining points are interpolated with cubic interpolation). The error map showing the difference between the interpolated and measured data is given in Fig. 14(b); the error is less than 0.2 G or about 1% of local BC value. Fig. 14(c) plots the relative errors of the reconstructed B_y distribution along the x-axis and z-axis, where errors are smaller than 0.15% and 0.01%, respectively, suggesting that the small interpolated BC errors has little effect on the reconstruction.

VI. Conclusion

We have presented a novel method to reconstruct the MFD in the 3-D working space of an EMS. Unlike other methods developed for design analysis, the coupled measurement–calculation does not require the knowledge of the magnetic structure, and thus, provides a cost-effective means to obtain physically accurate MFD outside the physical regions of the magnets.

The method, which solves the Laplace's equation (of a magnetic scalar potential in the working space) with the normal components of the magnetic flux density as BCs, has been illustrated with two application examples: a PM-based spherical

motor and an electromagnetic flowmeter. The method has also been validated by comparing the reconstructed MFD against measured data, and both comparisons show excellent agreements (with maximum errors of 3.6% and 0.52% for the motor and flowmeter, respectively).

The effect of reduced BC points on the reconstructed MFD has been discussed. As illustrated, a nearly identical MFD (with a relative error of less than 0.15%) can be contained illustrating the feasibility of reduced BC points for MFD reconstruction. This finding suggests that an effective method to select measured BC points can be based on gradient information, and that it is desirable to develop a real-time method capable of selecting measured points without any knowledge of the BC morphology—an interesting but challenging research topic being explored.

The ability to reconstruct physically accurate MFDs offers a rational basis for model validation, force/torque calculation, system identification, and parameter estimation that are essential for model-based motion control of a spherical motor, sensitivity prediction (dry calibration) of an electromagnetic flowmeter, etc. The reconstruction method can be extended to other physical field-based mechatronics systems. For example, a thermal or electrical field obeys similar governing equations (such as Laplace and Poisson equations), and has measurable DBC and NBC.

REFERENCES

[1] H. Son and K.-M. Lee, "Distributed multipole models for design and control of PM actuators and sensors," *IEEE/ASME Trans. Mechatronics*, vol. 13, no. 2, pp. 228–238, Apr. 2008.

[2] D. V. Lee and S. A. Velinsky, "Analysis and experimental verification of a three-dimensional noncontacting angular motion sensor," *IEEE/ASME Trans. Mechatronics*, vol. 13, no. 6, pp. 612–622, Dec. 2007.

[3] S. K. Cho, H. Z. Jin, J. M. Lee, and B. Yao. (2009, Mar. 4). Teleoperation of a mobile robot using a force-reflection joystick with sensing mechanism of rotating magnetic field, *IEEE/ASME Trans. Mechatronics* [Online]. DOI: 10.1109/TMECH.2009.2013848.

[4] X. Shan, S.-K. Kuo, J. Zhang, and C.-H. Menq, "Ultra precision motion control of a multiple degrees of freedom magnetic suspension stage," *IEEE/ASME Trans. Mechatronics*, vol. 7, no. 1, pp. 67–78, Mar. 2002.

[5] M. Komori and T. Yamane, "Magnetically levitated micro PM motors by two types of active magnetic bearings," *IEEE/ASME Trans. Mechatronics*, vol. 6, no. 1, pp. 43–49, Mar. 2001.

[6] E. H. Maslen, D. T. Montie, and T. Iwasaki, "Robustness limitations in self-sensing magnetic bearings," *ASME J. Dyn. Syst., Meas. Control*, vol. 128, no. 2, pp. 197–203, 2006.

[7] X. Fu, L. Hu, J. Zou, H. Y. Yang, X. D. Ruan, and C. Y. Wang, "Divisionally analytical reconstruction of the magnetic field around an electromagnetic velocity probe," *Sens. Actuators A*, vol. 150, no. 1, pp. 12–23, 2009.

[8] X. Z. Zhang and J. Hemp, "Measurement of pipe flow by an electromagnetic probe," *ISA Trans.*, vol. 33, pp. 181–184, 1994.

[9] B. Horner, F. Mesch, and A. Trachtler, "A multi-sensor induction flowmeter reducing errors due to non-axisymmetric flow profiles," *Meas. Sci. Technol.*, vol. 7, no. 3, pp. 354–360, 1996.

[10] D. M. Sousa and G. D. Marques, "Study of the air gap magnetic field distribution of a nuclear magnetic resonance iron-core magnet," in *Proc. IEEE Region 8 Conf. Comput. Technol. Electr. Electron. Eng. (SIBIRCON 2008)*, pp. 242–247.

[11] L. Yan, I.-M. Chen, G. Yang, and K.-M. Lee, "Analytical and experimental investigation on the magnetic field and torque of a permanent magnet spherical actuator," *IEEE/ASME Trans. Mechatronics*, vol. 11, no. 4, pp. 409–419, Aug. 2006.

[12] L. Hu, J. Zou, X. Fu, Y. H. Yang, X. D. Ruan, and C. Y. Wang, "A reconstruction approach to determining the magnetic field around an electromagnetic velocity probe," *Meas. Sci. Technol.*, vol. 20, pp. 015103-1–015103-7, 2009. DOI:10.1088/0957-0233/20/1/015103.

[13] K.-M. Lee and C.-K. Kwan, "Design concept development of a spherical stepper for robotic applications," *IEEE Trans. Robot. Autom.*, vol. 7, no. 1, pp. 175–181, Feb. 1991.

[14] W. Wang, J. Wang, G. W. Jewell, and D. Howe, "Design and control of a novel spherical permanent magnet actuator with three degrees of freedom," *IEEE/ASME Trans. Mechatronics*, vol. 8, no. 4, pp. 457–468, Dec. 2003.

[15] K.-M. Lee, K. Bai, and J. Lim, "Dipole models for forward/inverse torque computation of a spherical motor," *IEEE/ASME Trans. Mechatronics*, vol. 14, no. 1, pp. 46–54, Feb. 2009.

[16] K.-M. Lee, R. A. Sosseh, and Z. Wei, "Effects of the torque model on the control of a VR spherical motor," *IFAC Control Eng. Practice*, vol. 12, no. 11, pp. 1437–1449, 2004.

[17] D.-H. Kim, S.-H. Lee, I.-H. Park, and J.-H. Lee, "Derivation of a general sensitivity formula for shape optimization of 2-D magnetostatic systems by continuum approach," *IEEE Trans. Magn.*, vol. 38, no. 2, pp. 1125–1128, Mar. 2002.

[18] K. P. Prokopidis, N. V. Kantartzis, and T. D. Tsiboukis, "Performance optimization of the PML absorber in lossy media via closed-form expressions of the reflection coefficient," *IEEE Trans. Magn.*, vol. 39, no. 3, pp. 1234–1237, May 2003.

[19] L. Yan, I.-M. Chen, C.-K. Lim, G. Yang, W. Lin, and K.-M. Lee, "Design and analysis of a permanent magnet spherical actuator," *IEEE/ASME Trans. Mechatronics*, vol. 13, no. 2, pp. 239–248, Apr. 2008.

[20] K.-M. Lee, R. Roth, and Z. Zhou, "Dynamic modeling and control of a ball-joint-like VR spherical motor," *ASME J. Dyn. Syst., Meas. Control*, vol. 118, no. 1, pp. 29–40, 1996.

[21] J. A. Shercliff, *The Theory of Electromagnetic Flow-Measurement*. Cambridge, U.K.: Cambridge Univ. Press, 1962.

Liang Hu received the B.Eng. degree in 2004 from the Department of Mechanical Engineering, Zhejiang University, Hangzhou, China, where he is currently working toward the Ph.D. degree.

His current research interests include flow measurement and instrumentation, and measurement and computation of magnetic field.

Kok-Meng Lee (M'89–SM'02–F'05) received the B.S. degree from the State University of New York, Buffalo, in 1980, and the S.M. and Ph.D. degrees from Massachusetts Institute of Technology, Cambridge, in 1982 and 1985, respectively.

He is currently a Professor in the Woodruff School of Mechanical Engineering, Georgia Institute of Technology, Atlanta. His current research interests include system dynamics/control, robotics, automation, and mechatronics. He holds eight patents in machine vision, 3-DOF spherical motor/encoder, and live-bird handling system.

Prof. Lee is a Fellow of the American Society of Mechanical Engineers. He received the National Science Foundation Presidential Young Investigator Award, the Sigma Xi Junior Faculty Research Award, the International Hall of Fame New Technology Award, and the Kayamori Best Paper Award.

Xin Fu received the B.Eng. degree from Chengdu University of Science and Technology, Chengdu, China, in 1982, the M.Eng. degree from Southwest Agricultural University, Chongqing, China, in 1990, and the Ph.D. degree from the University of Leoben, Leoben, Austria, in 1999.

Since 1999, he has been with Zhejiang University, Hangzhou, China, where he was the Director of the State Key Laboratory of Fluid Power Transmission and Control from 2005 to 2009 and is currently a Professor and the Vice-Dean of the Department of Mechanical Engineering. His current research interests include microfluidic technology, simulation and visualization of flow field, fluid vibration and noise control, and flow measurement and instrumentation.